HHS Public Access

Author manuscript

Biochemistry. Author manuscript; available in PMC 2017 May 24.

Published in final edited form as:

Biochemistry. 2016 May 24; 55(20): 2864–2874. doi:10.1021/acs.biochem.6b00343.

Probing the Role of Active Site Water in the Sesquiterpene Cyclization Reaction Catalyzed by Aristolochene Synthase

Mengbin Chen[†], **Wayne K. W. Chou**[‡], **Naeemah Al-Lami**[§], **Juan A. Faraldos**[§], **Rudolf K. Allemann**[§], **David E. Cane**[‡], and **David W. Christianson**[†,#,*]

[†]Roy and Diana Vagelos Laboratories, Department of Chemistry, University of Pennsylvania, Philadelphia, Pennsylvania 19104-6323, United States

[‡]Department of Chemistry, Brown University, Box H, Providence, Rhode Island 02912-9108, United States

[§]School of Chemistry, Cardiff University, Park Place, Cardiff CF10 3AT, United Kingdom

[#]Radcliffe Institute for Advanced Study and Department of Chemistry and Chemical Biology, Harvard University, Cambridge, Massachusetts 02138, United States

Abstract

Aristolochene synthase (ATAS) is a high-fidelity terpenoid cyclase that converts farnesyl diphosphate exclusively into the bicyclic hydrocarbon aristolochene. Previously-determined crystal structures of ATAS complexes revealed trapped active site water molecules that could potentially interact with catalytic intermediates: water "w" hydrogen bonds with S303 and N299, water molecules "w1" and "w2" hydrogen bond with Q151, and a fourth water molecule is coordinated to the Mg^{2+}_{c} ion. There is no obvious role for water in the ATAS mechanism, since the enzyme exclusively generates a hydrocarbon product. Thus, these water molecules are tightly controlled so that they cannot react with carbocation intermediates. Steady-state kinetics and product distribution analyses of eight ATAS mutants designed to perturb interactions with active site water molecules (S303A, S303H, S303D, N299A, N299L, N299A/S303A, Q151H, and Q151E) indicate relatively modest effects on catalysis but significant effects on sesquiterpene product distributions. X-ray crystal structures of S303A, N299A, N299A/S303A, and Q151H mutants reveal minimal perturbation of active site solvent structure. Seven of the eight mutants generate farnesol and nerolidol, possibly resulting from addition of the Mg^{2+}_{c}-bound water molecule to the initially formed farnesyl cation, but no products are generated that would suggest enhanced reactivity of other active site water molecules. However, intermediate germacrene A tends to accumulate in these mutants. Thus, apart from the possible reactivity ofMg^{2+}_{c}-bound water, active site water molecules in ATAS are not directly involved in the chemistry of catalysis,

[*]To whom correspondence should be addressed to: Roy and Diana Vagelos Laboratories, Department of Chemistry, University of Pennsylvania, 231 South 34th Street, Philadelphia, PA, 19104-6323. Tel: 215-898-5714; ; Email: chris@sas.upenn.edu

Accession Codes

The atomic coordinates and crystallographic structure factors of the S303A ATAS-**4** complex, the N299A ATAS-FSPP complex, the N299A ATAS-**4** complex, the N299A/S303A ATAS-**4** complex, and the Q151H ATAS-FSPP complex have been deposited in the Protein Data Bank (www.rcsb.org) with accession codes 5IMI, 5IVG, 5IMP, 5IMN, and 5IN8, respectively.

Notes

The authors declare no competing financial interest.

but instead contribute to the template that governs the conformation of the flexible substrate and carbocation intermediates.

The structural and stereochemical diversity of terpenoids, including steroids and carotenoids, is unmatched by any other family of natural products, in that more than 75,000 different terpenoids have been discovered to date. Terpenoids serve countless biological functions in all domains of life, and many are utilized as pharmaceuticals, fragrances, flavors, and fuels.[1] The first committed step in terpenoid biosynthesis is typically the conversion of an achiral isoprenoid precursor, such as C_{10} geranyl diphosphate, C_{15} farnesyl diphosphate, or C_{20} geranylgeranyl diphosphate, into a cyclic or polycyclic hydrocarbon with structural and stereochemical precision.[2-4] Hydrocarbon cyclization products are subsequently modified, e.g., through oxidation, acetylation, benzoylation, glycosylation, etc., by additional enzymes to generate biologically active terpenoids.[5]

Class I terpenoid cyclases initiate the cyclization of an isoprenoid diphosphate by triggering substrate ionization to yield an allylic cation and inorganic pyrophosphate. Despite low amino acid sequence identities among class I terpenoid cyclases from different domains of life, these cyclases share the characteristic α-helical fold first identified in avian farnesyl diphosphate synthase.[6] The active site of a class I terpenoid cyclase is flanked by two signature metal binding motifs: the aspartate-rich segment DDXX(D,E) and the NSE motif (N,D)DXX(S,T)XX(R,K)E.[7-9] Amino acid side chains in these motifs coordinate to three divalent metal ions together with the substrate diphosphate group, and these metal coordination interactions induce conformational changes that enclose the active site and shield it from bulk solvent prior to substrate ionization.[10,11]

The active site of a terpenoid cyclase is typically lined by hydrophobic aliphatic and aromatic residues, comprising a three-dimensional template that binds the flexible substrate and chaperones carbocation intermediates through a specific sequence of carbon-carbon bond-forming reactions.[12-14] The volume of a terpenoid cyclase active site is often just slightly larger than the volume of the isoprenoid substrate, so as to ensure a snug fit between the template and the flexible isoprenoid substrate.[15,16] In such circumstances, most if not all active site water molecules are sterically displaced by substrate binding. This also provides chemical protection for catalysis, since an errant water molecule trapped in the active site could conceivably quench a carbocation intermediate.[17] Even so, some terpenoid cyclases generate alcohol products, indicating that capture of the final carbocation intermediate by water is an essential catalytic strategy.[18-21] Moreover, even in cyclases that do not generate alcohol products, trapped water molecules are occasionally observed in fully closed active sites complexed with analogues of the substrate, carbocation intermediates, or product.[22,23] Thus, a terpenoid cyclase must be able to control a trapped active site water molecule, when present, so that it reacts at the right time – or not at all – in the cyclization cascade.

The water management strategy in the active site of *Aspergillus terreus* aristolochene synthase (ATAS) is particularly intriguing. ATAS is a high fidelity cyclase that converts farnesyl diphosphate (FPP) exclusively into the sesquiterpene hydrocarbon (+)-aristolochene.[9,24] There is no obvious role for water in the ATAS mechanism: a 1,10-cyclization reaction leads to the formation of (*S*)-(–)-germacrene A, which undergoes

reprotonation to enable a 1,6-cyclization reaction that ultimately leads to formation of the bicyclic product (Figure 1a).[25] However, recent high resolution crystal structures of ATAS complexes with the unreactive substrate analogue farnesyl-*S*-thiolodiphosphate (FSPP) as well as aza analogues of carbocation intermediates reveal trapped active site water molecules in each complex studied (Figure 1b).[23] Conserved water molecule "w" forms a hydrogen bond with N213 (a Mg^{2+}_B ligand in the NSE motif), N299, and S303; this water molecule is conserved in all crystal structures of ATAS in the closed conformation regardless of the ligand bound in the active site.[23] On the opposite side of the active site, conserved water molecules "w1" and "w2" are additionally trapped and hydrogen bonded with Q151 in the upper side of the active site, adjacent to the DDXXD motif. Finally, a Mg^{2+}_C-bound water molecule is exposed to the upper active site. Since wild-type ATAS generates exclusively (+)-aristolochene and no hydroxylated products, all of these water molecules must be chemically inert in catalysis. Therefore, we hypothesize that these water molecules comprise an essential part of the active site contour which serves as the template for catalysis.

Here, we probe the role of active site water molecules in ATAS by perturbing their hydrogen bond partners S303, N299, and Q151 through site-directed mutagenesis, and characterizing the steady-state kinetics and product profiles of each mutant. Interpretation of these results in view of X-ray crystal structures of selected mutants reveals how the fidelity of FPP cyclization is influenced by active site water, even when no hydroxylated products are generated.

EXPERIMENTAL

Site-specific mutants of ATAS were prepared by PCR mutagenesis starting with the previously-reported[23] His_6-Δ12-ATAS plasmid; mutants were expressed and purified as previously reported with minor modifications. Briefly, LB medium (6 × 1 L) containing 100 μg/mL ampicillin and 34 μg/mL chloramphenicol was inoculated with a 5-mL starting culture and grown at 37 °C with aeration. Cells were induced with 0.05-0.3 mM isopropyl β-D-1-thiogalactopyranoside at 16 °C when the optical density at 600 nm reached 0.8-1.0. After expression for 18 h, cells were pelleted by centrifugation.

For each mutant, the cell pellet was resuspended in Ni-NTA wash buffer [50 mM K_2HPO_4 (pH 7.7), 300 mM NaCl, 10% (v/v) glycerol, and 3 mM tris(2-carboxyethyl)-phosphine hydrochloride (TCEP)]. Cells were lysed by sonication for 10-20 min. After centrifugation, cell debris was discarded and supernatant was loaded on a Ni-NTA column. Protein was eluted with a 0–400 mM imidazole gradient in Ni-NTA wash buffer. Occasionally, protein samples were additionally purified using a 10-mL HiTrap Q HP column (GE Healthcare) after exchange to Q wash buffer [10 mM Tris (pH 8.0) and 10 mM NaCl] when additional impurities were detected in some preparations. Elution was performed with a 0–500 mM NaCl gradient in Q wash buffer. Fractions were analyzed by SDS-PAGE, and the most active ones were combined, concentrated, and loaded onto a HiLoad 26/60 Superdex column (GE Healthcare) pre-equilibrated with 25 mM MES (pH 6.5), 150 mM NaCl, 2 mM $MgCl_2$, 10% (v/v) glycerol, and 3 mM TCEP. Final protein samples were 95-98% pure based on SDS-PAGE analysis.

Product assays were carried out in duplicate on a 5-mL scale using a previously described method with slight modifications.[26] Reactions were initiated at 30 °C by adding enzyme into assay buffer containing substrate FPP overlaid with 5 mL *n*-pentane. After 18-20 h of reaction, hydrocarbon products were extracted from the reaction mixture with three portions of *n*-pentane; extracts were run through anhydrous $MgSO_4$ to eliminate trace amounts of water. Samples were then concentrated under vacuum in an ice water bath using a rotary evaporator and analyzed by gas chromatography-mass spectrometry (GC-MS).

Gas chromatography-mass spectrometry (GC-MS) analyses were performed using an Agilent 5977A Series GC/MSD instrument (70 eV, electron impact), a 1-μL injection volume, and a 3 min solvent delay. Achiral GC-MS conditions used a temperature program with a 2 min hold at 60 °C, a 20 °C min^{-1} increment to 280 °C, followed by a 2 min hold at 280 °C, and a HP-5ms capillary column (0.25 mm ID × 30 m length × 0.25 mm film, Agilent Technologies). Chiral GC-MS conditions used a temperature program with a 2 min hold at 60 °C, a 3 °C min^{-1} increment to 220 °C, followed by a 2 min hold at 220 °C, and a CP-Chirasil-Dex CB capillary column (0.25 mm ID × 25 m length × 0.25 mm film, Agilent Technologies). Comparison of GC-MS detected compounds to their standards was done using the MassFinder 4.2.1 program (http://www.massfinder.com).

To examine how each mutation affected steady-state reaction kinetics, activity assays were conducted in triplicate on a 100-μL scale using a previously described method with slight modifications.[26] Purified ATAS mutants were incubated with FPP in 100 μL assay buffer [25 mM HEPES (pH 8.0) and 5 mM $MgCl_2$] at 30 °C. Concentrations and incubation times for each mutant were adjusted accordingly in order to measure initial reaction rates. Reactions were quenched by adding 30 μL 0.5 M ethylenediaminetetraacetic acid (EDTA) and products were extracted with 1 mL hexane twice. Extracts were passed through a 1-mL silica gel column, which was washed with 2 mL hexane followed by 1 mL hexane/ethyl ether (11:1). All eluates were collected in a scintillation vial containing 5 mL scintillation liquid. Radioactive counts were measured using a Beckman liquid scintillation counter. Control experiments were performed to determine background counts. Data were processed with Prism software.

For crystallography, FSPP was purchased from Echelon Biosciences Inc., and carbocation analogue **4** was synthesized as described.[23] Crystals of ATAS mutant complexes with these ligands were prepared by cocrystallization in sitting drops through the vapor diffusion method at 4 °C. Briefly, a 1-μL drop of protein solution [7-10 mg/mL ATAS mutant, 20 mM MES (pH 6.5), 1.9 mM $MgCl_2$, 120 mM NaCl, 3 mM TCEP, 1.6 mM sodium pyrophosphate, 1.5 mM ligand] was added to a 1-μL drop of precipitant solution and equilibrated against a 60-80 μL reservoir of precipitant solution. Different precipitant solutions were used for the crystallization of different mutants. For crystallization of the S303A ATAS-**4** complex, the precipitant solution was 200 mM NH_4OAc, 20% PEG 3350; for crystallization of the N299A ATAS-**4** complex, the precipitant solution was 200 mM $Mg(OAc)_2$, 20% PEG 3350; for crystallization of the N299A ATAS-FSPP complex, the precipitant solution was 200 mM $Mg(OAc)_2$, 20% PEG 3350; for crystallization of the N299A/S303A ATAS-**4** complex, the precipitant solution was 200 mM NaCl, 100 mM

HEPES (pH 7.5), 25% PEG 3350; for crystallization of Q151H ATAS with FSPP, the precipitant solution was 200 mM magnesium formate, 20% PEG 3350.

After growing to maximum dimensions, crystals of ATAS mutant-ligand complexes were gradually transferred to a cryoprotectant solution [20-25% (v/v) glycerol in mother liquor] and flash-cooled in liquid nitrogen. X-ray diffraction data were collected at beamline X29A of the National Synchrotron Light Source (Brookhaven National Laboratory), beamline 24-ID-C at the Advanced Photon Source (Argonne National Laboratory), and beamline 14-1 at Stanford Synchrotron Radiation Lightsource. X-ray diffraction data were processed using HKL2000.[27] Crystals of ATAS mutant-inhibitor complexes were isomorphous with the wild-type ATAS-FSPP complex, belonging to space group $P3_121$ with 4 monomers in the asymmetric unit.

Crystal structures of ATAS mutant-ligand complexes were solved by molecular replacement using Phaser for Molecular Replacement in the CCP4 package[28] with a monomer of wild-type ATAS (PDB accession code: 4KUX)[23] as a search probe. Iterative cycles of refinement and model building were performed with PHENIX and COOT, respectively.[29,30] Inhibitor, Mg^{2+} ions, and water molecules were added to each model in the later stages of refinement. Data collection and refinement statistics are recorded in Table 1.

RESULTS

S303A, S303H, and S303D ATAS

The 2.46 Å-resolution X-ray crystal structure of S303A ATAS complexed with bicyclic carbocation intermediate analogue **4** is essentially identical to that of the wild-type ATAS-**4** complex,[23] with a root-mean-square (rms) deviation of 0.31 Å for 285 Cα atoms between the two structures (Figure 2). Water molecule "w" remains in the same position observed in the wild-type enzyme despite the loss of the hydrogen bond with S303, and it remains hydrogen bonded with N213 and N299. Although the conformations of active site residues are essentially identical between the two structures, the 6-membered ring of **4** bearing the isopropylidene group tends toward a sofa-like conformation slightly different from the chair-like conformation observed in the wild-type enzyme.[23] This difference may be a consequence of the lower resolution structure of S303A ATAS, since the structure of the wild-type ATAS-**4** complex was determined at 1.95 Å resolution. At 2.46 Å resolution, the position of the isopropylidene substituent of **4** in the S303 ATAS complex is only moderately well defined in the electron density map (Figure 2a).

The lack of any major structural differences between S303A ATAS and wild-type ATAS is consistent with similar steady-state kinetic parameters measured for these enzymes (Table 2). However, the mutant enzyme exhibits slightly compromised cyclization fidelity, in that it generates 88.5% aristolochene (Figure 3). Two minor products identified are the cyclization intermediate germacrene A (9.5%), which reflects the loss of effective general acid catalysis to reprotonate this initially formed cyclic terpene, and nerolidol (2%), which indicates that the initially formed farnesyl cation can be immediately quenched by an active site water molecule.

That this quenching reaction can compete, albeit weakly, with the C1-C10 bond-forming reaction leading to germacrene A suggests that the position and orientation of C10 is slightly compromised in S303A ATAS. In the structure of the ATAS-FSPP complex (Figure 1b),[23] the C10 atom of FSPP abuts water molecule "w". Weakening hydrogen bond interactions with water molecule "w" in S303A ATAS may weaken the template that holds C10 in place. If so, water molecule "w" is an essential part of the template that governs the conformation of the flexible substrate.

Although we were unable to crystallize S303H ATAS and S303D ATAS, steady-state kinetic parameters indicate that the consequences of these sterically-demanding mutations are much more severe, with approximately 10- and 250-fold reductions in catalytic efficiency (Table 2). Interesting, too, is the fact that these mutants generate diminished amounts of aristolochene (32.9% and 15.8%, respectively). These mutants also generate a greater percentage of the hydroxylated products nerolidol as well as farnesol, with total hydroxylated product percentages of 10.5% and 47.4% for S303H ATAS and S303D ATAS, respectively (Figure 3). Nerolidol and farnesol are generated by the addition of water to the initially formed allylic cation upon FPP ionization. Increased percentages of these sesquiterpene alcohols generated by S303H ATAS and S303D ATAS are similarly consistent with defects in the active site template that would otherwise hold the C1 and C10 atoms of FPP close together for the initial cyclization reaction.

Based on analysis of the active site solvent structure in the ATAS-FSPP complex[23] (Figure 1b), the Mg^{2+}_{C}-bound water molecule is located directly over the plane of the incipient allylic cation that would result from FPP ionization. Although the Mg^{2+}_{C}-bound water molecule appears to be poised for stereospecific addition to C3 to yield 3*R*-nerolidol or to C1 to generate farnesol, chiral GC-MS analysis established that the nerolidol generated by S303D ATAS and other mutants is a completely racemic mixture of the 3*R* and 3*S* stereoisomers. In some fraction of the mutant proteins, the initially-generated allylic cation must be sufficiently disordered so as to allow addition of water to either side of the allylic cation in place of the normal electrophilic cyclization by intramolecular attack on C10. Since the Mg^{2+}_{C}-bound water molecule is closest to the C1 and C3 atoms of the farnesyl group in the ATAS-FSPP complex[23], we suggest that this water molecule is responsible for the generation of hydroxylated products.

N299A, N299V, and N299L ATAS

The 1.95 Å-resolution structure of N299A ATAS complexed with substrate analogue FSPP showed that all residues lining the active site adopt essentially identical conformations with those in wild-type ATAS-FSPP structure (Figure 4). The void created by substituting N299 with alanine is partially occupied by water molecule "w4", which corresponds to the former position of the Nδ atom of N299. The orientation of the isopropylidene group of FSPP differs slightly from that observed in the wild-type active site. However, given that 99.5% of the hydrocarbon products generated by N299A ATAS are cyclic (Figure 3), it appears that the N299A substitution does not significantly perturb the ability to achieve the reaction geometry required for the 1,10-cyclization reaction.

The 2.04 Å-resolution structure of N299A ATAS complexed with carbocation analogue **4** reveals the binding of two additional water molecules, "w3" and "w4", in locations corresponding to the positions formerly occupied by the Oδ and Nδ atoms of N299 (Figure 5). Additionally, the side chain of Y61 flips by approximately 90° and makes van der Waals contacts with **4**. The binding conformation of **4** is similar to that observed in the wild-type enzyme,[23] but the analogue is tilted by approximately 20° so that the isopropylidene group points toward A299. It is interesting that the conformation of Y61, as influenced by the N299A substitution, impacts product outcome: mutants in which Y61 is flipped are defective in the step required to protonate germacrene A. Y61 is not the general acid that protonates germacrene A, given that the corresponding tyrosine-to-phenylalanine mutant of *Penicillium roqueforti* aristolochene synthase exhibits only a minor decrease in the catalytic efficiency of aristolochene production (the two aristolochene synthases are related by 57% sequence identity and their active site contours are essentially identical).[24] However, Y61 can nonetheless influence catalysis as discussed further in the next section.

Although the N299V ATAS protein was soluble and formed a dimer as indicated by gel filtration chromatography, no terpene products could be detected from incubation of FPP. We were also unable to crystallize this mutant. N299L ATAS was similarly difficult to work with, and was particularly susceptible to aggregation. We were unable to measure steady-state kinetics from this mutant; upon further investigation, we discovered that its melting temperature of 29.1 °C was just below the temperature of 30 °C at which kinetic assays were performed. We were able, however, to measure sesquiterpene product arrays generated by incubation of N299L ATAS with FPP (Figure 3). Here, too, the small percentage of nerolidol generated by N299L ATAS is racemic, indicative of sufficient substrate disorder following ionization to enable addition of water with equal facility to either side of the allylic cation.

N299A/S303A ATAS

The 2.52 Å-resolution structure of the double mutant N299A/S303A ATAS complexed with carbocation analogue **4** reveals that significant unoccupied volume is introduced around the mutated side chains, but no ordered water molecules are observed in the electron density map (Figure 6). It is nonetheless likely that this cavity is occupied by at least 3 water molecules, as observed in the structure of the N299A ATAS-**4** complex (Figure 5). Active site solvent molecules in the N299A/S303A ATAS-**4** complex are perhaps rendered invisible to crystallographic detection by disordered binding and/or the moderate resolution of the structure determination.

Interestingly, the mutation of N299 and S303 simultaneously is more synergistic than additive with regard to germacrene A production, which accounts for 72.5% of all products formed (Figure 3). Thus, the reprotonation of germacrene A in the ATAS mechanism is severely compromised in the double mutant. Catalytic efficiency (k_{cat}/K_M) is diminished approximately 20-fold compared with wild-type ATAS (Table 2). The additional active site volume introduced by the double mutation also compromises the template function of the active site, which, while still able to promote the initial C1-C10 bond-forming reaction that generates germacrene A, is no longer effective in precisely orienting this intermediate for normal protonation and cyclization to form the eudesmane cation.

In this structure, too, the side chain of Y61 is flipped approximately 90° to accommodate the isopropylidene group of **4**, with which it makes several van der Waals contacts (Figure 6). On the other hand, no van der Waals interactions are observed between Y61 and **4** in the wild-type ATAS-**4** complex[23] or the S303A ATAS-**4** complex (Figure 3). Interestingly, the conformational change of Y61 is observed in the wild-type enzyme upon the binding of a stereochemically-incorrect aza analogue – specifically, the enantiomer of **4** – so the conformational change of Y61 may signal the possibility of an aberrant cyclization cascade.[23] Taken together, we suggest that the conformation of Y61 in these mutants significantly influences the position and conformation of germacrene A. If template features specifically required for germacrene A cyclization are compromised, then germacrene A cyclization will not proceed.

Q151H and Q151E ATAS

The 2.35 Å-resolution structure of Q151H ATAS cocrystallized with FSPP reveals several surprising features in the active site (Figure 7). First, while water molecule ‘w2’ is absent, the carboxylate group of D84 points away from its usual orientation to form a hydrogen bond with water ‘w1’, with the Oδ atom of D84 forming a van der Waals contact with $N\varepsilon_2$ of H151. This interaction compromises the metal coordination environment such that only $Mg^{2+}{}_B$ and $Mg^{2+}{}_C$ are observed; moreover, $Mg^{2+}{}_C$ is no longer coordinated by D84, but instead drifts to a position approximately 2 Å away where it is coordinated by 6 water molecules with octahedral geometry in chain A (Figures 7a, 7b). Accordingly, this structure represents a snapshot of metal association/dissociation in a terpenoid cyclase active site.

Second, only one (thio)phosphate group is observed in the electron density map of chains A, C, and D, but the electron density map reveals an intact (thio)diphosphate group in chain B (Figures 7c, 7d). Some discontinuous, weak electron density peaks (< 3σ) are present in the active site pocket, but they are not readily interpretable as either the farnesyl group of FSPP or a derived hydrocarbon product. Possibly, the FSPP molecule was sufficiently reactive under the conditions of cocrystallization utilized for this variant to yield hydrocarbon and inorganic (thio)diphosphate products. However, we cannot explain why such reactivity would have been observed in this mutant but not in the wild-type enzyme,[23] or in N299A ATAS (Figure 4). Additionally, we cannot explain the appearance of the tetrahedral anion interpreted as inorganic (thio)phosphate, since neither phosphate nor sulfate were included in the crystallization buffer, unless the (thio)diphosphate product is susceptible to hydrolysis under the crystallization conditions utilized for this study.

Regardless of these unusual structural results, Q151H ATAS generates a broad mixture of aristolochene, germacrene A, farnesol, and racemic nerolidol, with no particularly dominant product and a catalytic efficiency only one order of magnitude lower than that of the wild-type enzyme (Figure 3, Table 2). As previously concluded for S303A and N299A mutants, the generation of hydroxylated products farnesol and racemic nerolidol by Q151H ATAS reflects the quenching of the initially formed farnesyl cation by a nearby water molecule, such as the $Mg^{2+}{}_C$-bound water.

A significant change in product distribution is observed for Q151E ATAS (Figure 3). Increased production of germacrene A indicates that the template function of the active site

is compromised, such that germacrene A does not undergo reprotonation to generate the eudesmane cation. Moreover, the generation of increased percentages of farnesol and racemic nerolidol by this mutant indicates that the competing rate of premature quenching of the initially formed farnesyl cation is comparable to the rate of the C1-C10 bond forming reaction.

DISCUSSION

A terpenoid cyclase is the archetype of a template-directed enzyme, in which the particular products generated are a function of the specific conformation of the flexible isoprenoid substrate imposed by the enzyme active site. In essence, the directions for substrate folding and the ensuing sequence of carbon-carbon bond-forming reactions are encoded by the active site contour. Aliphatic and aromatic amino acid side chains that typically define the active site contour play critical roles in the template function of a terpenoid cyclase. Curiously, polar side chains occasionally serve this function, too, and such side chains can be hydrogen bonded with trapped solvent molecules in the enzyme-substrate complex.

The structural and functional studies reported herein represent the first steps in dissecting structure-function relationships for polar amino acid side chains that contribute to the active site contour of ATAS, specifically, side chains that form hydrogen bonds with trapped solvent molecules at the periphery of the active site. Crystal structures of S303A ATAS and N299A ATAS show that water molecule "w" remains in place despite the deletion of one of its hydrogen bond interactions (Figures 2, 4, and 5). Only in the crystal structure of the double mutant, S303A/N299A ATAS, are no ordered solvent molecules observed (Figure 6), although this is probably a consequence of the slightly more modest resolution (2.52 Å) of the crystal structure determination. The Q151H substitution replaces one polar side chain with a larger polar side chain, which results in a ~2 Å movement of Mg^{2+}_{c} (no longer coordinated by protein residues, but instead by 6 water molecules), the conformational change of former Mg^{2+}_{c} ligand D84, and the steric displacement of water molecule w2.

Interestingly, crystal structures of N299A ATAS and S303A/N299A ATAS reveal that deleting the N299–Y61 hydrogen bond results in a ~90° rotation of the Y61 side chain. The side chain of Y61 is located in the region of the active site that accommodates the terminal isoprenoid moiety of FPP. Thus, Y61 plays an important role in directing the stereochemistry of C1-C10 bond formation and accordingly the stereochemistry of the derived isopropylidene group. Mutagenesis of N299, which forms a hydrogen bond with Y61, results in some loss of conformational control, such that the cyclization reaction is mostly aborted upon formation of germacrene A. This indicates that the 90° rotation of the Y61 side chain hinders the ability of germacrene A to be reprotonated by a general acid to enable eudesmane cation formation. The altered binding orientations of analogue **4** in the active site of N299A ATAS (Figure 5) and S303A/N299A ATAS (Figure 6) presumably reflect the loss of conformational control in the active sites of these mutant enzymes, which in turn leads to increased product diversity (Figure 3).

It is notable that the ATAS mutants studied generate only farnesol and nerolidol as hydroxylated products, indicating that water molecules "w", "w1", and "w2" (and "w3" and

"w4" in N299A ATAS) are located in positions such that they cannot readily react with carbocation intermediates. These catalytically inert water molecules appear to serve a more important function as part of the active site template, making van der Waals interactions with the substrate and carbocation intermediates. Active site water molecules have been observed from time to time in the closed active site conformations of terpenoid cyclases containing bound analogues, such as bornyl diphosphate synthase[22] and ATAS.[23] Thus, active site water is not inherently deleterious to catalysis by a terpenoid cyclase. The catalytic power of a terpenoid cyclase is not only rooted in its ability to direct the formation of myriad cyclization products from a common substrate, but also its ability to direct – or in this case, to suppress – the reactivity of water as a solvent for organic synthesis.

How, then, does a terpenoid cyclase activate a water molecule for catalysis? Simple examples of such reactivity are evident in the generation of farnesol and racemic nerolidol by the ATAS mutants reported herein: a Mg^{2+}_{c}-bound water molecule is closest to the incipient allylic cation and is probably the most likely nucleophile, based on the crystal structure of the ATAS-FSPP complex (Figure 1b).[23] If the C1-C10 bond forming step is compromised by mutagenesis, e.g., by altering the active site contour so that C10 is improperly oriented and/or the allylic cation is subject to conformational disorder upon its formation, then the Mg^{2+}_{c}-bound water molecule might be able to quench the newly formed farnesyl cation at C1 or C3.

When the allylic cation is quenched at C3 to form nerolidol, a racemic mixture results, indicating that the addition of water takes place in essentially an achiral environment. However, simple acid- or divalent metal ion-catalyzed solvolysis of FPP normally generates a 3–4:1 mixture of nerolidol to farnesol,[31,32] and this ratio is not observed for any of the ATAS mutants studied (Figure 3). This suggests that the allylic cation is quenched before complete release from the ATAS active site. It is possible, too, that FPP may bind to ATAS mutants that generate nerolidol and farnesol in an alternative conformation to that observed in the active site of the wild-type enzyme[23] or N299A ATAS (Figure 4), and the alternative conformation may facilitate quenching of the allylic cation by Mg^{2+}_{c}-bound water or perhaps even by an alternative water molecule.

The Mg^{2+}_{c}-bound water molecules may mediate proton exchange between the active site and bulk solvent,[23] through which a solvent-derived deuteron is utilized to protonate the 6,7-double bond in the germacrene A intermediate.[33] However, neither a Mg^{2+}_{c}-bound water molecule nor the substrate diphosphate group is suitably oriented to protonate the established *re*-face of the 6,7-double bond of the intermediate germacrene A, as is evident from the position of the corresponding 6,7-double bond in the ATAS-FSPP complex.[23] This suggests that the germacrene A intermediate may undergo reorientation in the active site so as to enable reprotonation and formation of the eudesmane cation. The structure of the complex between wild-type ATAS and the bicyclic aza analogue **4** suggests that the final stereospecific deprotonation generating the product aristolochene could be mediated by the PP_i counterion.[23]

Curiously, some cyclases contain polar and even charged residues in prominent active site positions. For example, methylisoborneol synthase contains a negatively charged glutamate

residue, E193, at the base of its active site. While E193 was initially hypothesized to orient an active site water molecule to quench the final carbocation intermediate, E193A, E193D, and E193L mutants exhibit no discernible changes in the yield of the hydroxylated product.[34] In contrast, the X-ray crystal structure of hedycaryol synthase accompanied by mutagenesis experiments suggests that D82 in the upper wall of the active site plays a role in activating a water molecule that quenches the final carbocation intermediate.[35] Similarly, the crystal structure of cineole synthase reveals that N338 hydrogen bonds with a water molecule at the base of the active site cleft; N338I cineole synthase does not generate hydroxylated products, thereby suggesting that N338 and its hydrogen bonded water molecule are critical for catalysis in the wild-type enzyme.[36]

In conclusion, the current study provides several key lessons regarding the role of water as both a solvent and a reagent for organic synthesis by a terpenoid cyclase. First, the $Mg^{2+}{}_{C}$-bound water molecule is the active site solvent molecule closest to the incipient allylic cation formed by FPP ionization. The reactivity of this bound solvent molecule might be facilitated by disorder of the farnesyl cation that results from the defects introduced into the active site contour of the mutant. Although the intrinsic nucleophilicity of this water would be reduced by complexation to Mg^{2+}, the latent reactivity of metal-bound water might be unmasked by the weakening of metal coordination or by the action of an unidentified proton acceptor. Such latent reactivity of $Mg^{2+}{}_{C}$-bound water may similarly be responsible for the generation of farnesol and/or nerolidol by other sesquiterpene cyclases as well. Second, terpenoid cyclase active site cavities are not always completely anhydrous when they form enzyme-substrate complexes and may occasionally contain trapped water molecules. These water molecules can be utilized in catalysis only if they are positioned to add to the empty 2*p* orbitals of carbocation intermediates. Otherwise, such water molecules simply comprise part of the active site contour, and as such will help govern the conformation of the flexible substrate and carbocation intermediates. Finally, in enzymes that have evolved to use water as a reagent for organic synthesis, some such as methylisoborneol synthase have no clearly defined general base to orient or activate a catalytic water molecule, and others such as hedycaryol synthase or cineole synthase do have a well-defined general base. Future studies with ATAS and other terpenoid cyclases will continue to illuminate the complexities of water management in terpenoid biosynthesis.

ACKNOWLEDGMENTS

We thank the National Synchrotron Light Source, Beamline X-29 (Brookhaven National Laboratory), the Stanford Synchrotron Radiation Lightsource, Beamline 14-1, and the Northeast Collaborative Access Team beamline 24-ID-C at the Advanced Photon Source (Argonne National Laboratory) for access to X-ray crystallographic data collection facilities.

Funding

This research was supported by U.S. NIH Grants GM56838 to D.W.C. and GM30301 to D.E.C., and by the Biotechnology and Biological Sciences Research Council (BBSRC) of the United Kingdom through grants BB/H01683X/1 and BB/G003572/1 to R.K.A.

ABBREVIATIONS

ATAS	*Aspergillus terreus* aristolochene synthase
FPP	farnesyl diphosphate
FSPP	farnesyl thiolodiphosphate
TCEP	tris(2-carboxyethyl)phosphine hydrochloride
HEPES	4-(2-hydroxyethyl)-1-piperazineethanesulfonic acid
GC-MS	gas chromatography-mass spectrometry
EDTA	ethylenediaminetetraacetic acid

REFERENCES

1. Gershenzon J, Dudareva N. The function of terpene natural products in the natural world. Nat. Chem. Biol. 2008; 3:408–414. [PubMed: 17576428]
2. Wendt KU, Schulz GE. Isoprenoid biosynthesis: manifold chemistry catalyzed by similar enzymes. Structure. 1998; 6:127–133. [PubMed: 9519404]
3. Davis, EM.; Croteau, R. Biosynthesis: aromatic polyketides, isoprenoids, alkaloids. Vol. 209. Springer-Verlag berlin; Berlin: 2000. Cyclization enzymes in the biosynthesis of monoterpenes, sesquiterpenes, and diterpenes; p. 53-95.
4. Christianson DW. Structural biology and chemistry of the terpenoid cyclases. Chem. Rev. 2006; 106:3412–3442. [PubMed: 16895335]
5. Lange BM, Croteau R. Genetic engineering of essential oil production in mint. Curr. Opin. Plant Biol. 1999; 2:139–144. [PubMed: 10322195]
6. Tarshis LC, Yan M, Poulter CD, Sacchettini JC. Crystal structure of recombinant avian farnesyl diphosphate synthase at 2.6-Å resolution. Biochemistry. 1994; 33:10871–10877. [PubMed: 8086404]
7. Chen A, Kroon PA, Poulter CD. Isoprenyl diphosphate synthase: Protein sequence comparisons, a phylogenetic tree, and predictions of secondary structure. Protein Sci. 1994; 3:600–607. [PubMed: 8003978]
8. Rynkiewicz MJ, Cane DE, Christianson DW. Structure of trichodiene synthase from *Fusarium sporotrichioides* provides mechanistic inferences on the terpene cyclization cascade. Proc. Natl. Acad. Sci. USA. 2001; 98:13543–13548. [PubMed: 11698643]
9. Cane DE, Kang I. Aristolochene synthase. Purification, molecular cloning, high-level expression in *Escherichia coli*, and characterization of the *Aspergillus terreus* cyclase. Arch. Biochem. Biophys. 2000; 376:354–364. [PubMed: 10775423]
10. Aaron JA, Christianson DW. Trinuclear metal clusters in catalysis by terpenoid synthases. Pure Appl. Chem. 2010; 82:1585–1597. [PubMed: 21562622]
11. van der Kamp MW, Sirirak J, Zurek J, Allemann RK, Mulholland AJ. Conformational change and ligand binding in the aristolochene synthase catalytic cycle. Biochemistry. 2013; 52:8094–8105. [PubMed: 24106830]
12. Starks CM, Back K, Chappell J, Noel JP. Structural basis for cyclic terpene biosynthesis by tobacco 5-epi-aristolochene synthase. Science. 1997; 277:1815–1820. [PubMed: 9295271]
13. Wendt KU, Poralla K, Schulz GE. Structure and function of a squalene cyclase. Science. 1997; 277:1811–1815. [PubMed: 9295270]
14. Lesburg CA, Zhai G, Cane DE, Christianson DW. Crystal structure of pentalene synthase: mechanistic insights on terpenoid cyclization reactions in biology. Science. 1997; 277:1820–1824. [PubMed: 9295272]

15. Rynkiewicz MJ, Cane DE, Christianson DW. X-ray crystal structures of D100E trichodiene synthase and its pyrophosphate complex reveal the basis for terpene product diversity. Biochemistry. 2002; 41:1732–1741. [PubMed: 11827517]
16. Köksal M, Jin Y, Coates RM, Croteau R, Christianson DW. Taxadiene synthase structure and evolution of modular architecture in terpene biosynthesis. Nature. 2011; 469:116–120. [PubMed: 21160477]
17. Pronin SV, Shenvi RA. Synthesis of highly strained terpenes by non-stop tail-to-head polycyclization. Nat. Chem. 2012; 4:915–920. [PubMed: 23089866]
18. Kawaide H, Hayashi K, Kawanabe R, Sakigi Y, Matsuo A, Natsume M, Nozaki H. Identification of the single amino acid involved in quenching the *ent*-kauranyl cation by a water molecule in *ent*-kaurene synthase of *Physcomitrella patens*. FEBS J. 2011; 278:123–133. [PubMed: 21122070]
19. Cane DE, Watt RM. Functional expression and mechanistic characterization of a germacradienol synthase from *Streptomyces coelicolor* implicated in geosmin synthase. Proc. Natl. Acad. Sci. USA. 2003; 100:1547–1551. [PubMed: 12556563]
20. Wang C-M, Cane DE. Biochemistry and molecular genetics of the biosynthesis of the earthy odorant methylisoborneol in *Streptomyces coelicolor*. J. Am. Chem. Soc. 2008; 130:8908–8909. [PubMed: 18563898]
21. Nakano C, Kudo F, Eguchi T, Ohnishi Y. Genome mining reveals two novel bacterial sesquiterpene cyclases: (–)-germacradien-4-ol and (–)-epi-α-bisabolol synthases from *Streptomyces citricolor*. ChemBioChem. 2011; 12:2271–2275. [PubMed: 23106076]
22. Whittington DA, Wise ML, Urbansky M, Coats RM, Croteau RB, Christianson DW. Bornyl diphosphate synthase: Structure and strategy for carbocation manipulation by a terpenoid cyclase. Proc. Natl. Acad. Sci. U. S. A. 2002; 99:15375–15380. [PubMed: 12432096]
23. Chen M, Al-lami N, Janvier M, D'Antonio EL, Faraldos JA, Cane DE, Allemann RK, Christianson DW. Mechanistic insights from the binding of substrate and intermediate analogues to aristolochene synthase. Biochemistry. 2013; 52:5441–5453. [PubMed: 23905850]
24. Felicetti B, Cane DE. Aristolochene synthase: Mechanistic analysis of active site residues by site-directed mutagenesis. J. Am. Chem. Soc. 2004; 126:7212–7221. [PubMed: 15186158]
25. Cane DE, Prabhakaran PC, Salaski EJ, Harrison PHM, Noguchi H, Rawlings BJ. Aristolochene biosynthesis and enzymatic cyclization of farnesyl pyrophosphate. J. Am. Chem. Soc. 1989; 111:8914–8916.
26. Li R, Chou WKW, Himmelberger JA, Litwin KM, Harris GG, Cane DE, Christianson DW. Reprogramming the chemodiversity of terpenoid cyclization by remolding the active site contour of epi-isozizaene synthase. Biochemistry. 2014; 53:1155–1168. [PubMed: 24517311]
27. Otwinowski, Z.; Minor, W. Processing of X-ray diffraction data collected in oscillation mode. In: Carter, CW., Jr.; Sweet, RM., editors. Methods in Enzymology. Macromolecular Crystallography (Part A). Vol. 276. Academic Press; New York: 1997. p. 307-326.
28. McCoy AJ, Grosse-Kunstleve RW, Adams PD, Winn MD, Storoni LC, Read RJ. Phaser crystallographic software. J. Appl. Cryst. 2007; 40:658–674. [PubMed: 19461840]
29. Adams PD, Afonine PV, Bunkoczi G, Chen VB, Davis IW, Echols N, Headd JJ, Hung L-W, Kapral GJ, Grosse-Kunstleve RW, McCoy AJ, Moriarty NW, Oeffner R, Read RJ, Richardson DC, Richardson JS, Terwilliger TC, Zwart PH. PHENIX: a comprehensive Python-based system for macromolecular structure solution. Acta Cryst. 2010; 66:213–221.
30. Emsley P, Cowtan K. Coot: model-building tools for molecular graphics. Acta Cryst. 2004; 60:2126–2132.
31. Miller DJ, Gao J, Truhlar DG, Young NJ, Gonzalez V, Allemann RK. Stereochemistry of eudesmane cation formation during catalysis by aristolochene synthase from *Penicillium roqueforti*. Org. Biomol. Chem. 2008; 6:2346–2354. [PubMed: 18563268]
32. Rittersdorf W, Cramer F. Die Hydrolyse von Phosphaten and Pyrophosphaten Einiger Monoterpenalkohole. Tetrahedron. 1967; 23:3015–3022.
33. George-Nascimento C, Pont-Lezicka R, Cori O. Nonenzymic formation of nerolidol from farnesyl pyrophosphate in the presence of bivalent cations, *Biochem*. Biophys. Res. Commun. 1971; 45:119–124.

34. Köksal M, Chou WKW, Cane DE, Christianson DW. Structure of 2-methylisoborneol synthase from *Streptomyces coelicolor* and implications for the cyclization of a noncanonical *C*-methylated monoterpenoid substrate. Biochemistry. 2012; 51:3011–3020. [PubMed: 22455514]

35. Baer P, Rabe P, Citron CA, de Oliveira Mann CC, Kaufmann N, Groll M, Dickschat JS. Hedycaryol synthase in complex with nerolidol reveals terpene cyclase mechanism. ChemBioChem. 2014; 15:213–216. [PubMed: 24399794]

36. Kampranis SC, Ioannidis D, Purvis A, Mahrez W, Ninga E, Katerelos NA, Anssour S, Dunwell JM, Degenhardt J, Makris AM, Goodenough PW, Johnson CB. Rational conversion of substrate and product specificity in a *Salvia* monoterpene synthase: structural insights into the evolution of terpene synthase function. Plant Cell. 2007; 19:1994–2005. [PubMed: 17557809]

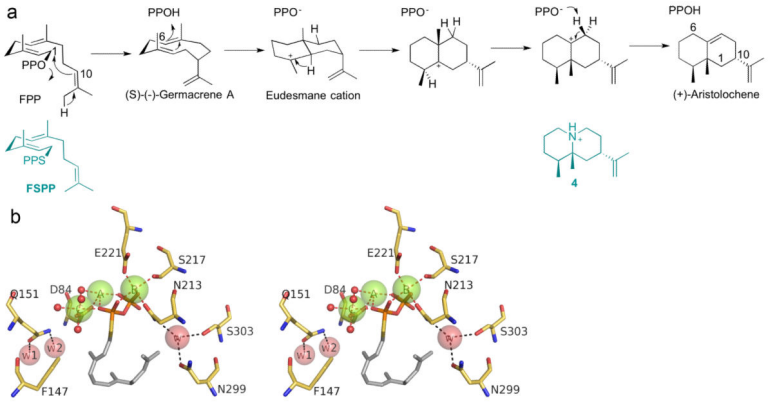

Figure 1.

(a) Cyclization of farnesyl diphosphate (FPP) as catalyzed by *A. terreus* aristolochene synthase (ATAS). The diphosphate leaving group (OPP) may serve as a general base-general acid during the cyclization cascade. Also shown are the unreactive substrate analogue farnesyl-*S*-thiolodiphosphate (FSPP) and the aza analogue of the final carbocation intermediate (**4**; numbering scheme established by Chen and colleagues[23]). (b) Stereoview showing the structure of the ATAS-FSPP complex (chain A).[23] Conserved Mg^{2+}_{c}-bound water molecules, as well as active site water molecules w, w1, and w2, are represented by their approximate van der Waals radii. Atomic color-codes are as follows: C = light brown (protein) or gray (FSPP), N = blue, O = red, P = orange, S = yellow; Mg^{2+} = green spheres, selected Mg^{2+}-bound water molecules = small red spheres, water molecules w, w1, and w2 = large pink spheres. Hydrogen bond interactions between these water molecules and Q151, N213, N299, and S303 are indicated by dashed lines.

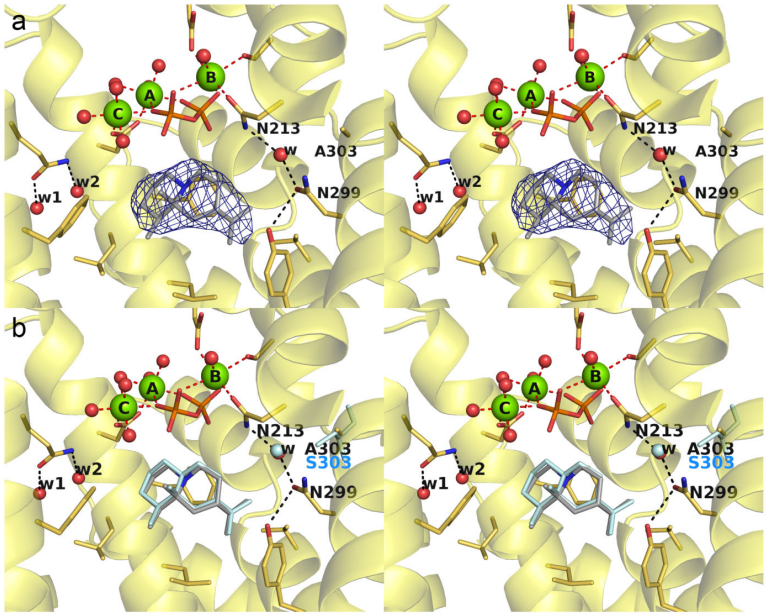

Figure 2.

(a) Simulated annealing omit map of the S303A ATAS-**4** complex (chain A, contoured at 3.0 σ). Atoms are color-coded as follows: C = yellow (protein) or gray (**4**), O = red, N = blue, P = orange, Mg^{2+} ions = green spheres, solvent molecules = red spheres. Hydrogen bonds and metal ion coordination interactions are shown as black and red dashed lines, respectively; hydrogen bonds with the PP_i group are omitted for clarity. (b) Superposition of the S303A ATAS-**4** complex (color-coded as in (a)) with S303, water molecule w, and aza analogue **4** as observed in the wild-type ATAS-**4** complex.[23]

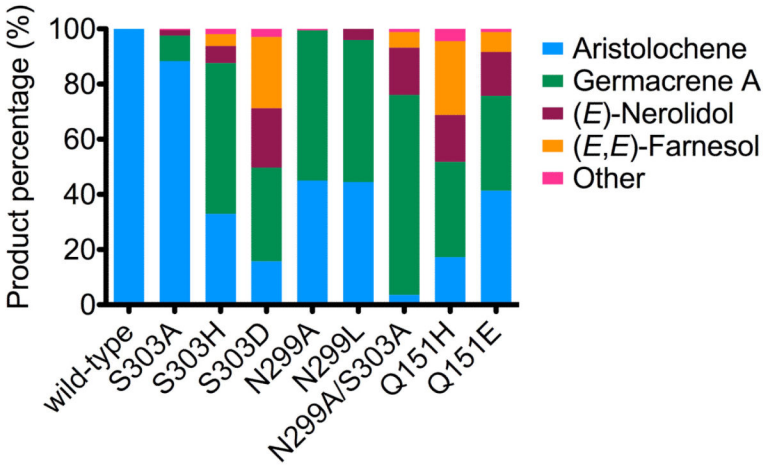

Figure 3.

Sesquiterpene product distributions generated by ATAS mutants. The exclusive formation of aristolochene by the wild-type enzyme was previously reported by Felicetti and Cane.[24]

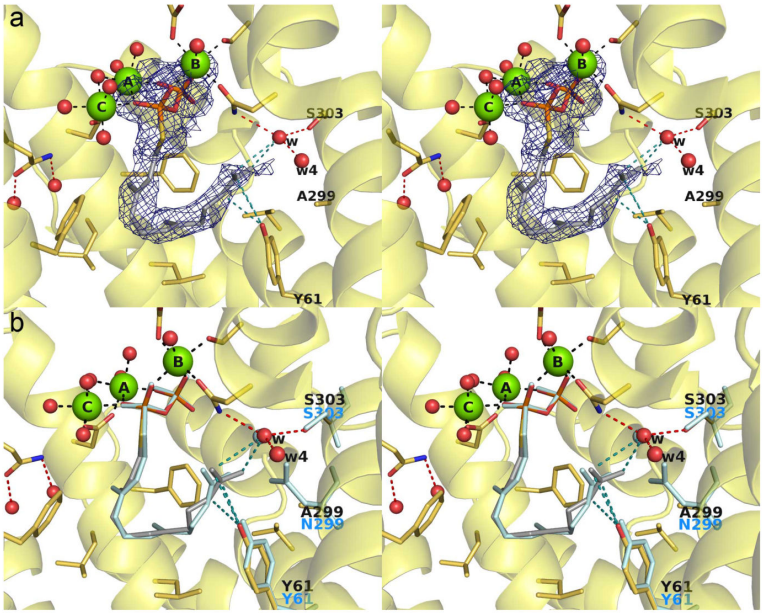

Figure 4.

(a) Simulated annealing omit map of the N299A ATAS-FSPP complex (chain A, contoured at 2.5 σ). Atoms are color-coded as follows: C = yellow (protein) or gray (FSPP), O = red, N = blue, P = orange, Mg^{2+} ions = green spheres, solvent molecules = red spheres. Hydrogen bonds and metal ion coordination interactions are shown as black and red dashed lines, respectively; hydrogen bonds with the PP_i group are omitted for clarity. (b) Superposition of the N299A ATAS-FSPP complex (color-coded as in (a)) with S303, N299, Y61, water molecule w, and FSPP as observed in the wild-type ATAS-FSPP complex.[23]

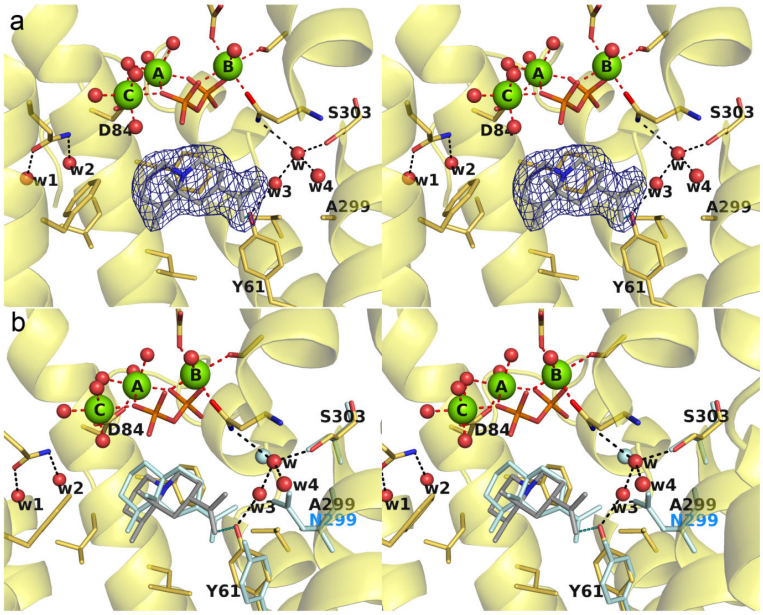

Figure 5.

(a) Simulated annealing omit map of the N299A ATAS-**4** complex (chain A, contoured at 3.0 σ). Atoms are color-coded as follows: C = yellow (protein) or gray (**4**), O = red, N = blue, P = orange, Mg^{2+} ions = green spheres, solvent molecules = red spheres. Hydrogen bonds and metal ion coordination interactions are shown as black and red dashed lines, respectively; hydrogen bonds with the PP_i group are omitted for clarity. (b) Superposition of the N299A ATAS-**4** complex (color-coded as in (a)) with N299, Y61, water molecule w, and aza analogue **4** as observed in the wild-type ATAS-**4** complex.[23]

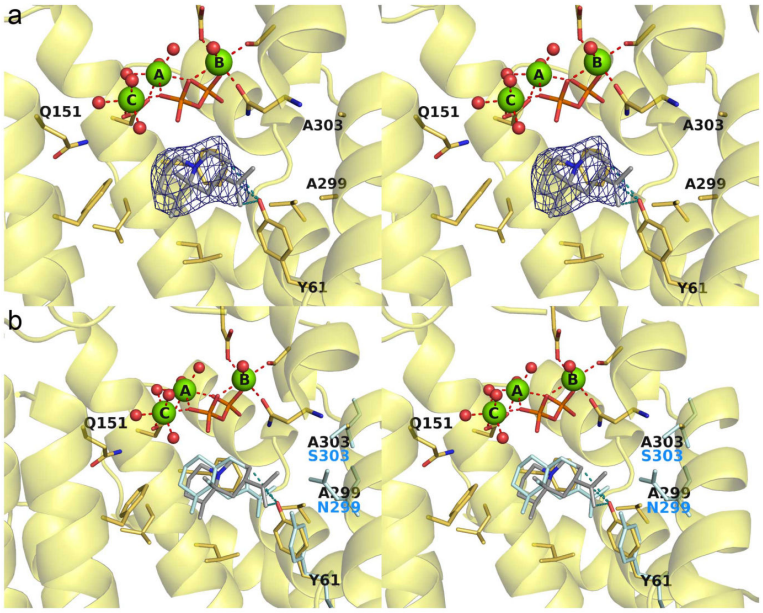

Figure 6.

(a) Simulated annealing omit map of the S303A/N299A ATAS-**4** complex (chain A, contoured at 3.0 σ). Atoms are color-coded as follows: C = yellow (protein) or gray (**4**), O = red, N = blue, P = orange, Mg^{2+} ions = green spheres, solvent molecules = red spheres. Hydrogen bonds and metal ion coordination interactions are shown as black and red dashed lines, respectively; hydrogen bonds with the PP_i group are omitted for clarity. Note that active site water molecules are not observed in this structure, possibly due to its modest 2.52 Å resolution. (b) Superposition of the S303A/N299A ATAS-**4** complex (color-coded as in (a)) with S303, N299, Y61, and aza analogue **4** as observed in the wild-type ATAS-**4** complex.[23]

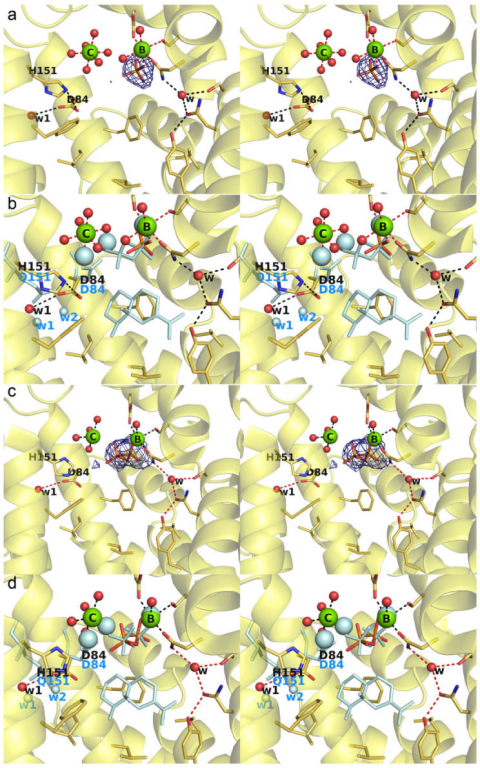

Figure 7.

(a) Simulated annealing omit map (contoured at 3.0 σ) of the (thio)phosphate ion (P_i) observed in chain A of Q151H ATAS cocrystallized with the unreactive substrate analogue FSPP (P_i is also observed in the active sites of chains C and D). Atoms are color-coded as follows: C = yellow (protein) or gray (**4**), O = red, N = blue, P = orange, Mg^{2+} ions = green spheres, solvent molecules = red spheres. Hydrogen bonds and metal ion coordination interactions are shown as black and red dashed lines, respectively. (b) Superposition of chain A of Q151H ATAS cocrystallized with FSPP (color-coded as in (a)) with Q151, D84, 3 Mg^{2+} ions, diphosphate group, and aza analogue **4** as observed in the wild-type ATAS-**4** complex. (c) Simulated annealing omit map (contoured at 3.0 σ) of the (thio)diphosphate ion (P_i) observed in chain B of Q151H ATAS cocrystallized with the unreactive substrate analogue FSPP. (d) Superposition of chain B of Q151H ATAS cocrystallized with FSPP (color-coded as in (a)) with Q151, D84, 3 Mg^{2+} ions, diphosphate group, and aza analogue **4** as observed in the wild-type ATAS-**4** complex.[23] The orientation of the diphosphate group has changed in response to changes in Mg^{2+} ion positions.

Table 1

Data collection and refinement statistics

Complex	S303A ATAS-4	N299A ATAS-FSPP	N299A ATAS-4	N299A/S303A ATAS-4	Q151H ATAS-FSPP
Beamline	NSLS X29A	NSLS X29A	NSLS X29A	APS 24IDC	SSRL 14-1
Resolution limits (Å)	50.0-2.46	50.0-1.95	50.0-2.04	50.0-2.52	50.0-2.35
Space group	$P3_121$	$P3_121$	$P3_121$	$P3_121$	$P3_121$
Unit cell parameters *a*, *c* (Å)	124.13, 203.41	123.41, 203.46	123.85, 202.28	124.30, 202.63	122.85, 202.52
Total/unique reflections	922407 (66366)	2900523 (130703)	1956559 (114972)	476896 (61282)	689724 (73952)
Redundancy	13.9	22.2	17.0	7.8	9.3
R_{merge} [a,b]	0.184 (0.0)[c]	0.125 (0.0)[c]	0.111 (0.0)[c]	0.156 (0.0)[c]	0.183 (0.0)[c]
R_{pim} [a,d]	0.054 (0.401)	0.028 (0.246)	0.033 (0.405)	0.085 (0.775)	0.063 (0.679)
$CC_{1/2}$ [a,e]	0.935 (0.708)	0.977 (0.890)	0.934 (0.707)	0.875 (0.589)	0.826 (0.490)
$I/\sigma(I)$ [a]	19.7 (2.0)	31.4 (3.6)	24.7 (1.9)	14.8 (1.2)	17.7 (1.4)
Completeness (%) [a]	100.0 (99.9)	100.0 (100.0)	100.0 (100.0)	99.9 (99.9)	99.9 (100.0)
Reflections used in work set/test set	66303/2003	130628/2001	114883/2006	61228/1990	73914/2007
R_{work} [f]	0.215	0.162	0.203	0.195	0.211
R_{free} [f]	0.253	0.199	0.235	0.254	0.243
Protein atoms [g]	9883	9874	9849	9836	9903
Solvent atoms [g]	602	1372	999	288	705
Metal ions [g]	12	12	12	12	8
Pyrophosphate ions [g]	6	0	6	6	1
Phosphate ion [g]	0	0	0	0	3
Terpene analogues [g]	4	4	4	4	0
Glycerol molecules [g]	1	3	2	1	7
R.m.s. deviations					
Bonds (Å)	0.002	0.015	0.003	0.008	0.002
Angles (deg)	0.6	1.5	0.6	1.1	0.5
Average B factors (Å^2)					
Protein	51	36	42	58	51
Solvent	45	44	42	52	50
Ligands	56	40	39	57	67
Ramachandran Plot (%)					
Allowed	94.6	96.1	97.8	94.1	95.9

Complex	S303A ATAS-4	N299A ATAS-FSPP	N299A ATAS-4	N299A/S303A ATAS-4	Q151H ATAS-FSPP
Additionally allowed	5.4	3.9	2.1	5.9	4.1
Generously allowed	0.0	0.0	0.1	0.0	0.0
PDB accession code	5IMI	5IVG	5IMP	5IMN	5IN8

[a] Numbers in parentheses refer to the highest resolution shell of data.

[b] R_{merge} for replicate reflections, $R = \Sigma|I_h - \langle I_h \rangle|/\Sigma\langle I_h \rangle$; I_h = intensity measure for reflection h, $\langle I_h \rangle$ = average intensity for reflection h calculated from replicate data.

[c] R_{merge} values higher than 1.000 are reported as 0.000 by HKL2000; this is sometimes observed for datasets with high redundancy.

[d] $R_{pim} = \Sigma[1/(n\text{-}1)]^{1/2}|I_h - \langle I_h \rangle|/\Sigma\langle I_h \rangle$; n is the number of observations (redundancy).

[e] $CC_{1/2} = \sigma_\tau^2/(\sigma_\tau^2 + \sigma_\varepsilon^2)$, where σ_τ^2 is the true measurement error variance and $\sigma_\varepsilon 2$ is the independent measurement error variance.

[f] $R_{work} = \Sigma||F_o| - |F_c||/\Sigma|F_o|$ for reflections contained in the working set. $R_{free} = \Sigma||F_o| - |F_c||/\Sigma|F_o|$ for reflections contained in the test set held aside during refinement (5% of total). $|F_o|$ and $|F_c|$ are the observed and calculated structure factor amplitudes, respectively.

[g] Per asymmetric unit.

Table 2

Steady-state kinetic parameters for ATAS mutants

Mutant	k_{cat} (s^{-1})	K_M (μM)	k_{cat}/K_M ($M^{-1}s^{-1}$)
wild-type	0.027 ± 0.003	0.099 ± 0.05	2.7×10^5
S303A	0.045 ± 0.002	0.12 ± 0.02	3.7×10^5
S303H	0.0013 ± 0.0002	0.061 ± 0.02	2.1×10^4
S303D	0.00041 ± 0.00004	0.36 ± 0.09	1.1×10^3
N299A	0.012 ± 0.0004	0.41 ± 0.06	2.9×10^4
N299V[a]	---	---	---
N299L[b]	---	---	---
N299A/S303A	0.0058 ± 0.0003	0.41 ± 0.09	1.4×10^4
Q151H	0.00063 ± 0.0002	0.042 ± 0.01	1.5×10^4
Q151E	0.0015 ± 0.0006	0.10 ± 0.04	1.5×10^4

[a] N299V ATAS is soluble and exists as a dimer in solution, but we were unable to measure the generation of any terpenoid products.

[b] Although N299L ATAS suffers from compromised thermostability, and its tendency for aggregation hindered the measurement of steady-state kinetic parameters, this mutant generated sufficient sesquiterpene products for analysis as outlined in Figure 3.